MDPI

An Exploratory Study of MoS$_2$ as Anode Material for Potassium Batteries

Lucia Fagiolari [1,2,*], Daniele Versaci [1,2], Federica Di Berardino [1], Julia Amici [1,2], Carlotta Francia [1,2], Silvia Bodoardo [1,2] and Federico Bella [1,2,*]

[1] Department of Applied Science and Technology, Politecnico di Torino, Corso Duca degli Abruzzi 24, 10129 Torino, Italy

[2] National Interuniversity Consortium of Material Science and Technology, Via Giuseppe Giusti 9, 50121 Firenze, Italy

* Correspondence: lucia.fagiolari@polito.it (L.F.); federico.bella@polito.it (F.B.); Tel.: +39-011-090-4640 (L.F. & F.B.)

Abstract: Potassium-based batteries represent one of the emerging classes of post-lithium electrochemical energy storage systems in the international scene, due to both the abundance of raw materials and achievable cell potentials not far from those of lithium batteries. In this context, it is important to define electrodes and electrolytes that give reproducible performance and that can be used by different research groups as an internal standard when developing new materials. We propose molybdenum disulfide (MoS$_2$) as a valid anode choice, being a commercial and easily processable material, the 2D layered structure of which is promising for large potassium ions reversible storage. It has been proven to work for hundreds of cycles, keeping a constant specific capacity around 100 mAh g^{-1} while also preserving its electrochemical interphase and morphology.

Keywords: potassium battery; post-Li battery; molybdenum disulfide; anode; 2D electrode

1. Introduction

A suitable energy storage system is necessary to store the intermittent electricity produced by renewable resources and provide energy during down moments [1–5]. Nowadays, lithium-ion batteries (LIBs) are the best-known electrochemical energy storage systems in the market [6–10], due to their lightness, high operating voltage, high energy density and fast charge rate [11–15]. For these reasons, they currently dominate the market of electric vehicles and portable devices [16–20].

However, lithium is a limited resource, with a natural abundance of 0.0017% in the Earth crust [21] and this could threaten the further development of LIBs, due to the high cost. On the other hand, sodium and potassium are much more abundant in the Earth crust (2.3% and 1.5%, respectively) and can also be extracted from seawater [5]. In particular, potassium shows a potential value close to that of lithium in common cyclic carbonate-based organic solvents (–2.93 V vs. –3.04 V, referring to the standard hydrogen electrode) [22,23]. Conversely, sodium presents a more positive potential (i.e., –2.71 V); therefore, the exploitation of this alkaline metal in secondary batteries would bring to a 300 mV potential loss [24]. A second intriguing feature of potassium is that its cation (K$^+$) shows a weaker Lewis acidity than those of its Na$^+$ and Li$^+$ counterparts, therefore resulting in a smaller Stokes radius, higher ion mobility and lower desolvation energy in ester-based electrolytes [25–27]. On the other hand, K$^+$ possesses a bigger ionic radius than Li$^+$ and Na$^+$; thus, the materials developed for LIBs suffer from a huge structural reorganization when K$^+$ is intercalated/inserted [28]. For example, graphite, commonly used as an anode for LIBs, can reversibly host K$^+$ during the intercalation/deintercalation process, leading to the formation of KC$_8$ and a reversible capacity of 279 mAh g^{-1} [29–31]; however, it undergoes a severe volume expansion of 63%, six times higher with potassium than lithium,

leading to its detachment from the electrode surface after some cycles [32–34]. The huge expansion is also responsible for the exfoliation of the graphene layers and, consequently, the fast capacity decay. In this case, the ester-derived solid electrolyte interphase (SEI) layer is composed of a large fraction of organic species; it is not stable, is nonuniform and does not have the proper passivation effect on the graphite anode [35,36].

Nowadays, the research on suitable electrode materials for potassium-ion batteries (PIBs) is still at its infancy [37–40]. Up until now, carbon-based electrodes, alloying materials and transition metal dichalcogenides have been reported by different research groups [5,41–43]. Alloying anodes are elements of the V group (such as P, Sb and Sn) and show high theoretical capacity, since multiple electron reactions are often involved. However, they are subjected to a huge volumetric expansion, which causes the pulverization of the electrode material and capacity fading [44]. On the other hand, layered transition sulphides present an open 2D diffusion pathway, similar to that of graphite, but with a wider and tunable interlayer distance [20]. In this scenario, molybdenum disulfide (MoS_2) could represent a valid dichalcogenide anode for PIBs. In fact, it has a layered structure, in which the layers are stacked together by Van der Waals' interactions, its interlayer distance (0.62 nm) is suitable for alkali ion intercalation [45–47] and it ensures a theoretical capacity of 670 mAh g^{-1} [48]. In addition, in preliminary studies, it demonstrated a remarkable stability upon cycling, with more than a 95% retention efficiency after 150–200 cycles [20,21,25]. To the best of our knowledge, Ren et al. were the first who proposed MoS_2 for PIBs, showing that K^+ can be easily intercalated/deintercalated in the MoS_2 interlayer spaces, with the formation of $K_{0.4}MoS_2$ during the discharge process [20]. This hypothesis was subsequently confirmed by theoretical calculations [49]. In terms of electrochemical performances, the preliminary values of initial specific capacity were close to 98 mAh g^{-1}, of which only a contribution of 73 mAh g^{-1} was reversible, due to the formation of the SEI layer. Later on, the hybridization of MoS_2 with carbon-based materials was proposed as a simple strategy to solve the issue of low conductivity within the electrode matrix [21,25]. For example, Zhang et al. hybridized MoS_2 with carbon nanosheets grown onto nitrogen-doped graphene to avoid particle aggregation and boost conductivity values [21]; overall, they obtained a remarkable initial specific discharge capacity of 820 mAh g^{-1}, even if the initial Coulombic efficiency was still low due to the non-optimized SEI layer formation. Chong et al. reported a nanorose-like MoS_2 active material anchored onto the reduced graphene oxide, achieving a higher electrochemical performance with respect to the pristine counterpart [25].

Apart from the preliminary studies listed above, the scientific literature lacks a systematic investigation focused on the use of MoS_2 as an anode for PIBs. Indeed, when developing an emerging battery technology, it is necessary to define references for anodes, cathodes and electrolytes. In this paper, we show why MoS_2 could be a reasonable choice for PIBs by investigating the electrochemical performance of this active material and studying the mechanism behind its working principle through cyclic voltammetry (CV) and electrochemical impedance spectroscopy (EIS) experiments. We anticipate that MoS_2 showed a stable specific capacity of ≈100 mAh g^{-1} after a few cycles, while the initial phase of the galvanostatic test was characterized by an irreversible capacity loss attributed to the SEI layer formation and to parasitic reactions. The stability of the MoS_2 anode was remarkable and reproducible, with a 97.4% retention efficiency between the 100th and the 200th cycles. Overall, we hope that this paper can offer a benchmark for further investigations into transition layer dichalcogenides as anodic materials for PIBs.

2. Materials and Methods

MoS_2, potassium, potassium hexafluorophosphate (KPF_6), ethyl carbonate (EC) and diethyl carbonate (DEC) were purchased from Merck. Super C45 conductive carbon black (CB) and carboxymethyl cellulose sodium salt (Na-CMC) were purchased from Timcal and Daicel, respectively. All chemicals were used without any further purification step.

Electrodes were fabricated by mixing MoS_2, CB and Na-CMC (this latter was in a 5 wt% solution in Milli-Q water) at a weight ratio of 80:10:10. The latter was ball-milled at

30 Hz for 15 min in a ball mill (MM 400 Retsch), in order to obtain a homogeneous slurry. The obtained formulation was deposited onto a copper foil by doctor blade technique, using a 200 μm thick blade and an automatic film applicator (TQC Sheen B.V.) at a speed of 50 mm s^{-1}. The deposited paste was dried in air overnight. Disks with 15 (or 10 mm) diameter were cut by a die cutter and dried at 120 °C under vacuum for 4 h. The mass loading was ≈1.86 mg cm^{-2}. The X-ray diffraction (XRD) patterns of the electrode is shown in Figure S1 in the Supplementary Material. XRD was performed with a high-resolution Philips X'pert MPD powder diffractometer, equipped with Cu Kα radiation (V = 40 kV, I = 30 mA) and a curved graphite secondary monochromator

Electrochemical cells were assembled in an argon-filled glove box. The liquid electrolyte consisted of KPF$_6$ 0.80 M in EC:DEC (1:1, *v/v*). For galvanostatic charge/discharge cycles, the half-cell was assembled in coin architecture (LIR2032), using a potassium foil as a counter electrode. The two electrodes were separated by a glass microfiber separator (Whatmann, A/L, 0.64 mm thick), activated with ≈13 drops of the electrolyte solution and the cell was sealed by an automatic crimper (MSK-160E, MTI Corporation). A T cell configuration was employed for CV and EIS electrochemical characterization. In this case, electrode disks of 10 mm (diameter) were prepared, while potassium foils were used as both counter and reference electrodes; a glass microfiber separator (Whatmann, GF/A, 0.26 mm thick) was placed between the counter and the working electrodes.

CV was carried out between 0.01 and 3.0 V for five cycles, at a scan rate of 0.1, 0.05 and 0.5 mV s^{-1}. EIS was conducted in the frequency range between 100 kHz and 10 mHz, by applying an oscillating potential of 10 mV. CV and EIS experiment were carried out on a VSP3-e Biologic electrochemical workstation and data were processed by the EC-Lab® software. Galvanostatic charge/discharge tests were performed on an Arbin BT 2000 battery cycler instrument. Here, current density was varied between 0.05 and 5 A g^{-1}, considering the mass of the active material (MoS$_2$). All the above-mentioned electrochemical tests were performed at room temperature.

Field emission scanning electron microscopy (FESEM) was performed on an Auriga Zeiss Instrument (Carl Zeiss, Oberkochen, Germany). The cycled electrode was recovered from the cell and washed with the same solvent of the electrolyte solution to remove salts and any other product that would have compromised the quality of the images.

3. Results and Discussion

To investigate MoS$_2$ as an anodic material for PIBs, electrodes were fabricated by mixing the active material, a conductive additive (CB) and a binder (Na-CMC) in Milli-Q water. The carbon additive was necessary to provide electrical conductivity to the electrode. We decided to use CB C45 since it can be used in water-based formulations, thus avoiding the use organic solvents and lowering the environmental impact of the post-lithium batteries production.

With the aim of better evaluating the electrochemical behavior of the MoS$_2$ electrode, CV experiments were carried out. In the first cycle, the voltammogram (see Figure 1A) shows a cathodic branch featuring three peaks at 1.00, 0.28 and 0.01 V. In agreement with MoS$_2$-related studies in the field of post-lithium batteries [50,51], the peak at 1.00 V can be attributed to the intercalation of potassium ions into the MoS$_2$ interlayer space. This led to the formation of the K$_x$MoS$_2$ compound, with a theoretical capacity of 67 mAh g^{-1} [23]. The storage mechanism below 0.80 V was ascribed to the conversion reaction of MoS$_2$, being reduced to metallic molybdenum and K$_2$S. In the anodic branch of the CV trace, only one small broad peak was detected at around 1.60 V, which could be interpreted as the depotassiation process, also being present in the subsequent cycles. The anodic peak at 0.50 V could be related to the conductive carbon additive. The subsequent cycles (2nd–5th) almost overlapped the first one, indicating the rather good reversibility of the electrochemical process. Figure S2 in the Supplementary Material shows CV traces measured under different scan rates.
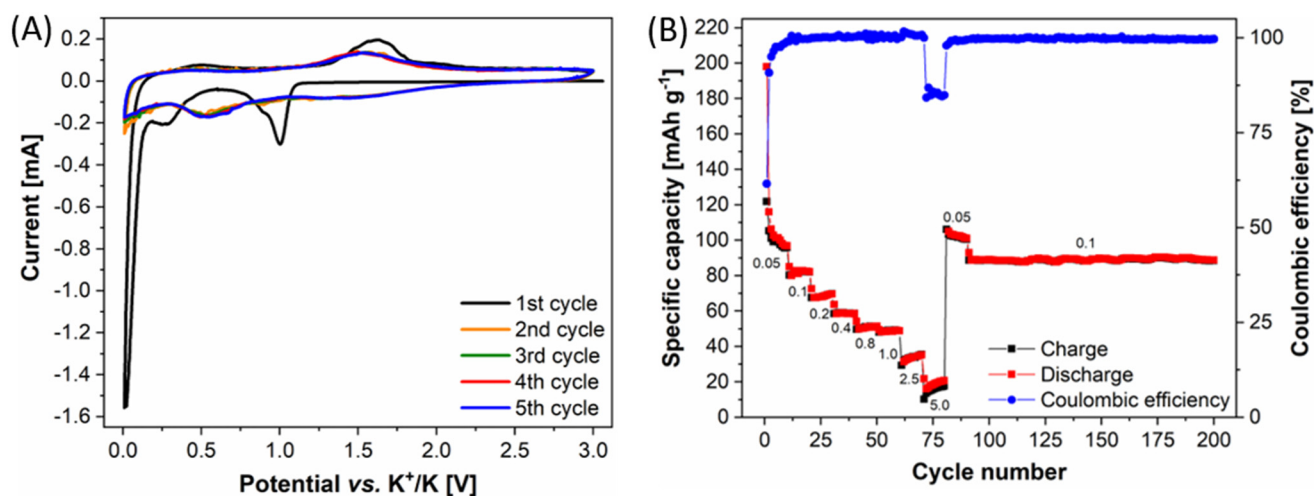
Figure 1. (**A**) Cyclic voltammogram (scan rate: 0.1 mV s^{-1}) obtained with a T cell configuration, using potassium metal foil as counter and reference electrodes and MoS$_2$ as working electrode. (**B**) Galvanostatic charge/discharge cycling of a coin cell based on the MoS$_2$ anode.

The electrochemical performance of the MoS$_2$ electrode was assessed by galvanostatic charge/discharge cycling, carried out at different current densities ranging from 0.05 to 5 A g^{-1}. The initial specific capacity was 200 mAh g^{-1} and reached 100–125 mAh g^{-1} in the first ten cycles, as reported in Figure 1B. The Coulombic efficiency of the first cycle was around 63%, which is similar to the values found in the literature for other PIB anodes [24]; then, it stabilized to 100% in a few cycles.

This initial irreversible capacity loss was mainly attributed to the formation of the SEI layer. Indeed, it has to be considered that we used a standard liquid electrolyte to make our results comparable with those present in the literature; moreover, the PIBs field has not yet defined an optimized electrolyte formulation (additives included) in the way it has already been established for LIBs, even if many studies are just starting to address this issue [52–55]. Upon cycling, specific capacity values stabilized and, when the current density was increased, these values slightly decreased, reaching 20 mAh g^{-1} at 5 A g^{-1}. In a later stage, when the applied current was shifted back to the initial value of 0.05 A g^{-1}, the cell fully recovered the initial specific capacity exceeding 100 mAh g^{-1}, highlighting the great electrochemical behavior of the MoS$_2$ electrode. When comparing the 100th and 200th cycles, the stability of our lab-scale cell is obvious, with an overall specific capacity retention of >97%. The stability of the electrochemical performance can also be noted in Figure 2A, in which charge/discharge profiles, i.e., potential vs. specific capacity curves, remain very close upon cycling, with a rather stable working potential window suggesting poor polarization phenomena. Figure 2B shows the charge/discharge profiles under the previously mentioned current regimes.

To get further insight, Figure S3 in the Supplementary Material shows charge-discharge profiles obtained at different current densities, while Figure S4 focuses on profiles related to the first 5 cycles at 0.05 A g^{-1}.

The morphology of the MoS$_2$ electrodes was investigated before and after 150 charge/discharge cycles; moreover, it was also carried out to know more about the SEI layer formation in the first cycles. Since the cycling performances are stable after the first few cycles, it can be realistically stated that the SEI layer does not vary in composition and thickness during charge/discharge process; therefore, post mortem FESEM could be a potential technique to investigate its morphology. The FESEM micrograph of the fresh electrode is shown in Figure 3A. It highlights the particle size in the micrometer range (lower than 5 μm, as confirmed in the commercial product datasheet and as also found in other literature studies using this material). The morphology showed a layered geometry, clearly visible in the micrograph. In regards to the conductive additive, it resulted in quite a homogeneous

distribution. On the other hand, the electrode obtained after cell disassembly was recovered and washed with the same solvent used for liquid electrolyte preparation (i.e., EC:DEC 1:1 *v/v*), with the aim of removing salts that would have compromised the quality of the images. The resulting micrograph (Figure 3B) shows similarities with those relative to the fresh electrode material. Indeed, MoS$_2$ particles remained in the micrometric size range and the morphology of the surface did not show any relevant difference. This is rather noteworthy, since the prolonged insertion/disinsertion of large potassium ions in the MoS$_2$-based anode could have damaged the electrode structure, as often occurs when studying anodes for post-lithium batteries [56,57].
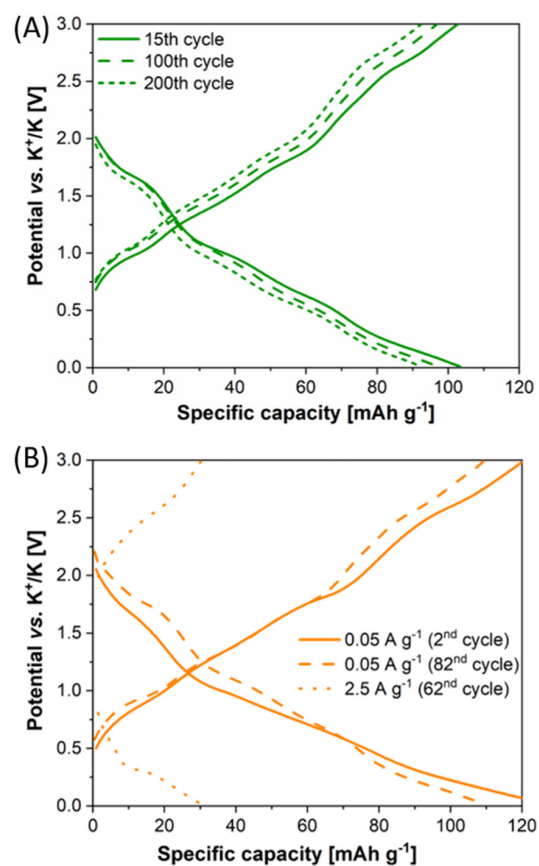

Figure 2. Potential vs. specific capacity profiles for a coin cell based on the MoS$_2$ anode: (**A**) Data collected at cycles no. 15, 100 and 200 and at a current density of 0.1 A g^{-1}; (**B**) Data collected at different current regimes and cell life.
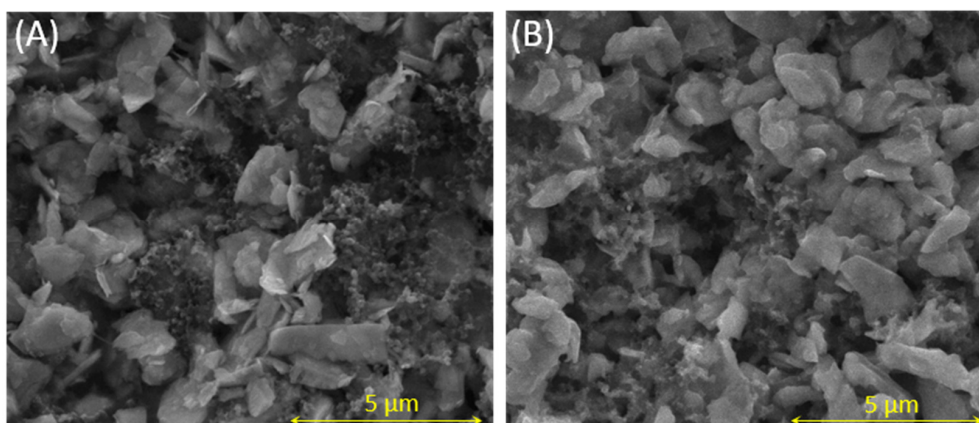
Figure 3. FESEM images at 10,000× of (**A**) fresh and (**B**) cycled MoS$_2$-based electrodes.

The forming stage was evaluated by recording the EIS spectra before and after the charge/discharge cycles. Figure 4A,B shows a first cycle profile typical of an electrode/electrolyte interphase that can be described—at first reading—by a semicircle and a straight line in the low-frequency region, which depicts the diffusion behavior; in any case, considering the slope quite different with respect to the theoretical 45°, it is not clearly excludable that the second part of the curve could be a wide semicircle. Starting from the second cycle, a depressed semicircle appeared at high and medium frequencies and another semi-circle was detected at the low-frequency region. Upon cycling, a straight line started to become evident, in particular at cycles 9–10. Overall, the shape of the EIS curves we recorded in a reproducible way is not so common for battery anodes; this will push us to carry out further studies, maybe coupled with in operando approaches to better clarify the occurring phenomena.
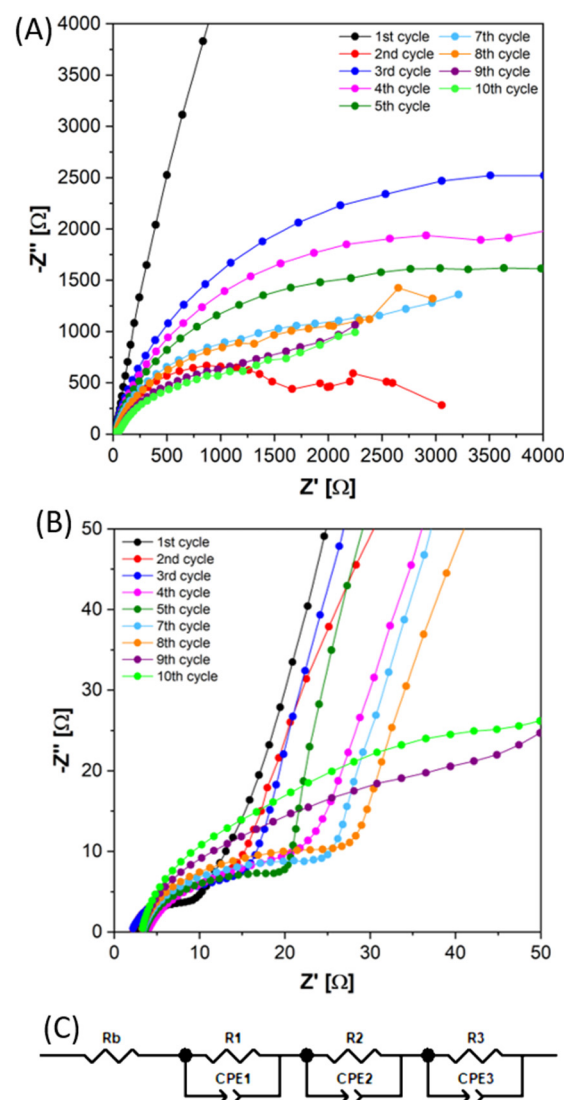
Figure 4. Nyquist plot for cells based on the MoS_2 anode: (**A**) Complete spectrum; (**B**) High frequency area. (**C**) Equivalent circuit used to fit the EIS spectra of MoS_2-based PIBs during the forming stage.

The equivalent circuit shown in Figure 4C was exploited to fit the obtained EIS spectra. The two semicircles detected in the spectra corresponded to the circuital elements R1-CPE1 and R2-CPE2. The third element represents the behavior at low frequencies. The values given by the fitting process are listed in Table 1. The bulk resistance, indicated with R_b, was rather stable and close to a value of 2.2–4.0 Ω. The R1 and R2 resistances increased, while R3 decreased. It is not straightforward to pinpoint the physical phenomena behind this

trend. Upon cycling, two interphases are formed: one was attributed to the SEI layer and the other to the conversion product. R3 could describe the charge transfer resistance, due to the semi-conductor material in the crystalline phase 1H-MoS_2. Our hypothesis is that the increase in R1 and R2 accompanies the gradual increase in the solid-state diffusion on potassium ions in the active material, while the decrease in R3 upon cycling indicates the lowering of charge transfer resistance during the cell operation. This finding has also been confirmed in a recent study dealing with MoS_2-based composite anodes for post-lithium batteries [58].

Table 1. R1, R2 and R3 values upon cycling.

Cycle	R1 [Ω]	R2 [Ω]	R3 [Ω]
3	4.11	9.41	5490
4	4.38	15.13	4320
7	9.02	11.58	2193
8	10.88	10.89	2259
10	13.31	40.18	1646

4. Conclusions

In conclusion, layered MoS_2 was tested as anodic material for PIBs and the resulting lab-scale prototypes proper functioning was investigated. The cells evidenced an irreversible loss of efficiency during the first cycles, due to the formation of the SEI layer and parasitic reactions. The use of an electrolyte additive to control this process is necessary and further analyses are required. Furthermore, after the initial loss, the specific capacity was $\approx$100 mAh g^{-1}. After the rate capability test in the range 0.05–5 A g^{-1}, the cell recovered its initial specific capacity and the stability was remarkable, with a 97.5% retention efficiency between the 100th and 200th cycles. CV, EIS and FESEM experiments supported the analysis of the electrochemical phenomena occurring with this electrode and its evolution upon time.

This preliminary investigation could offer a benchmark for the use of MoS_2 as an anode for PIBs: since the scientific literature is still in its infancy in this field, it is important to identify a cheap, stable and reproducible material that can be used as a reference when research groups develop new PIB electrodes and electrolytes. Moreover, further studies are needed to ameliorate the use of layered transition sulphides and, especially, their interaction with electrolytes (for which the introduction of specific additives is urgently required). Overall, upscalable, cheap and reproducible PIB materials will be a milestone to developing a reliable electrochemical energy storage system ready for integration with already-established sustainable photovoltaics [59–63].

Supplementary Materials: The following are available online at https://www.mdpi.com/article/10.3390/batteries8110242/s1, Figure S1: XRD pattern of commercial MoS_2 powder and MoS_2 after ball milling with C45 carbon additive, Na-CMC binder and water solvent; Figure S2: Cyclic voltammogram at different scan rates obtained with a T-cell configuration, using potassium metal foil as counter and reference electrodes, MoS_2 as working electrode and KPF_6 in EC:DEC 1:1 as the electrolyte; Fitted lines calculated from CV curves; Figure S3: Charge-discharge profiles at different current densities; Figure S4: Charge-discharge profiles in the first 5 cycles, obtained at 0.05 A g^{-1}. Reference [64] has been cited in Supplementary Materials.

Author Contributions: Conceptualization, L.F. and F.B.; methodology, L.F. and D.V.; investigation, L.F., D.V. and F.D.B.; resources, F.B., C.F. and S.B.; data curation, L.F., D.V. and F.D.B.; writing—original draft preparation, L.F. and F.D.B.; writing—review and editing, D.V., J.A., C.F. and F.B.; supervision, L.F., D.V. and F.B. All authors have read and agreed to the published version of the manuscript.

Data Availability Statement: The data presented in this study are available on request from the corresponding author.

Conflicts of Interest: The authors declare no conflict of interest.

References

1. Long, J.; Yang, Z.; Yang, F.; Cuan, J.; Wu, J. Electrospun core-shell Mn_3O_4/carbon fibers as high-performance cathode materials for aqueous zinc-ion batteries. *Electrochim. Acta* **2020**, *344*, 136155. [CrossRef]
2. Nederstedt, H.; Jannasch, P. Poly(*p*-phenylene)s tethered with oligo(ethylene oxide): Synthesis by Yamamoto polymerization and properties as solid polymer electrolytes. *Polym. Chem.* **2020**, *11*, 2418–2429. [CrossRef]
3. Wang, J.; Li, J.; He, X.; Zhang, X.; Yan, B.; Hou, X.; Du, L.; Placke, T.; Winter, M.; Li, J. A three-dimensional TiO_2-Graphene architecture with superior Li ion and Na ion storage performance. *J. Power Sources* **2020**, *461*, 228129. [CrossRef]
4. Li, L.; Deng, Y.; Chen, G. Status and prospect of garnet/polymer solid composite electrolytes for all-solid-state lithium batteries. *J. Energy Chem.* **2020**, *50*, 154–177. [CrossRef]
5. Liu, F.; Li, T.; Yang, Y.; Yan, J.; Li, N.; Xue, J.; Huo, H.; Zhou, J.; Li, L. Investigation on the Copolymer Electrolyte of Poly(1,3-dioxolane-*co*-formaldehyde). *Macromol. Rapid Commun.* **2020**, *41*, e2000047. [CrossRef]
6. Kou, Z.; Liu, C.; Miao, C.; Mei, P.; Yan, X.; Xiao, W. High-performance gel polymer electrolytes using P (VDF-HFP) doped with appropriate porous carbon powders as the matrix for lithium-ion batteries. *Ionics* **2020**, *26*, 1729–1737. [CrossRef]
7. González, F.; Garcia-Calvo, O.; Tiemblo, P.; García, N.; Fedeli, E.; Thieu, T.; Urdampilleta, I.; Kvasha, A. Synergy of inorganic fillers in composite thermoplastic polymer/ionic liquid/LiTFSI electrolytes. *J. Electrochem. Soc.* **2020**, *167*, 070519. [CrossRef]
8. Cao, X.; Cheng, J.; Zhang, X.; Zhou, D.; Tong, Y. Composite Polymer Electrolyte based on Liquid Crystalline Copolymer with High-temperature Stability and Bendability for All-solid-state Lithium-ion Batteries. *Int. J. Electrochem. Sci.* **2020**, *15*, 677–695. [CrossRef]
9. Yang, X.; Luo, J.; Sun, X. Towards high-performance solid-state Li–S batteries: From fundamental understanding to engineering design. *Chem. Soc. Rev.* **2020**, *49*, 2140–2195. [CrossRef]
10. Costa, C.M.; Lizundia, E.; Lanceros-Méndez, S. Review—Polymers for advanced lithium-ion batteries: State of the art and future needs on polymers for the different battery components. *Prog. Energy Combust. Sci.* **2020**, *79*, 100846. [CrossRef]
11. Boz, B.; Dev, T.; Salvadori, A.; Schaefer, J.L. Electrolyte and electrode designs for enhanced ion transport properties to enable high performance lithium batteries. *J. Electrochem. Soc.* **2021**, *168*, 090501. [CrossRef]
12. Zhang, D.; Tan, C.; Ou, T.; Zhang, S.; Li, L.; Ji, X. Constructing advanced electrode materials for low-temperature lithium-ion batteries: A review. *Energy Rep.* **2022**, *8*, 4525–4534. [CrossRef]
13. Eshetu, G.G.; Elia, G.A.; Armand, M.; Forsyth, M.; Komaba, S.; Rojo, T.; Passerini, S. Electrolytes and interphases in sodium-based rechargeable batteries: Recent advances and perspectives. *Adv. Energy Mater.* **2020**, *10*, 2000093. [CrossRef]
14. Chen, G.; Huang, J.; Gu, J.; Peng, S.; Xiang, X.; Chen, K.; Yang, X.; Guan, L.; Jiang, X.; Hou, L. Highly tough supramolecular double network hydrogel electrolytes for an artificial flexible and low-temperature tolerant sensor. *J. Mater. Chem. A* **2020**, *8*, 6776–6784. [CrossRef]
15. Wang, Z.; Liu, J.; Zhang, J.; Hao, S.; Duan, X.; Song, H.; Zhang, J. Novel chemically cross-linked chitosan-cellulose based ionogel with self-healability, high ionic conductivity, and high thermo-mechanical stability. *Cellulose* **2020**, *27*, 5121–5133. [CrossRef]
16. Gao, Y.; Pan, Z.; Sun, J.; Liu, Z.; Wang, J. High-Energy Batteries: Beyond Lithium-Ion and Their Long Road to Commercialisation. *Nano-Micro Lett.* **2022**, *14*, 94. [CrossRef]
17. Zaman, W.; Hatzell, K.B. Processing and manufacturing of next generation lithium-based all solid-state batteries. *Curr. Opin. Solid State Mater. Sci.* **2022**, *26*, 101003. [CrossRef]
18. Cheng, J.; Cao, X.; Zhou, D.; Tong, Y. Preparation of SiO_2 grafted polyimidazole solid electrolyte for lithium-ion batteries. *Ionics* **2020**, *26*, 3883–3892. [CrossRef]
19. Rao, J.; Wang, X.; Yunis, R.; Ranganathan, V.; Howlett, P.C.; MacFarlane, D.R.; Forsyth, M.; Zhu, H. A novel proton conducting ionogel electrolyte based on poly (ionic liquids) and protic ionic liquid. *Electrochim. Acta* **2020**, *346*, 136224. [CrossRef]
20. Shi, M.; Xiao, P.; Yang, C.; Sheng, Y.; Wang, B.; Jiang, J.; Zhao, L.; Yan, C.J. Scalable gas-phase synthesis of 3D microflowers confining MnO2 nanowires for highly-durable aqueous zinc-ion batteries. *J. Power Sources* **2020**, *463*, 228209. [CrossRef]
21. Xu, J.; Dou, S.; Cui, X.; Liu, W.; Zhang, Z.; Deng, Y.; Hu, W.; Chen, Y. Potassium-based electrochemical energy storage devices: Development status and future prospect. *Energy Storage Mater.* **2021**, *34*, 85–106. [CrossRef]
22. Meng, Y.; Nie, C.; Guo, W.; Liu, D.; Chen, Y.; Ju, Z.; Zhuang, Q. Inorganic cathode materials for potassium ion batteries. *Mater. Today Energy* **2022**, *25*, 100982. [CrossRef]
23. Lei, H.; Li, J.; Zhang, X.; Ma, L.; Ji, Z.; Wang, Z.; Pan, L.; Tan, S.; Mai, W. A review of hard carbon anode: Rational design and advanced characterization in potassium ion batteries. *InfoMat* **2022**, *4*, e12272. [CrossRef]
24. Tyagi, A.; Puravankara, S. Insights into the diverse precursor-based micro-spherical hard carbons as anode materials for sodium–ion and potassium–ion batteries. *Mater. Adv.* **2022**, *3*, 810–836.
25. Liu, Y.; Gao, C.; Dai, L.; Deng, Q.; Wang, L.; Luo, J.; Liu, S.; Hu, N. The features and progress of electrolyte for potassium ion batteries. *Small* **2020**, *16*, 2004096. [CrossRef]
26. Trano, S.; Corsini, F.; Pascuzzi, G.; Giove, E.; Fagiolari, L.; Amici, J.; Francia, C.; Turri, S.; Bodoardo, S.; Griffini, G.; et al. Lignin as Polymer Electrolyte Precursor for Stable and Sustainable Potassium Batteries. *ChemSusChem* **2022**, *15*, e202200294. [CrossRef]

27. Manarin, E.; Corsini, F.; Trano, S.; Fagiolari, L.; Amici, J.; Francia, C.; Bodoardo, S.; Turri, S.; Bella, F.; Griffini, G. Cardanol-Derived Epoxy Resins as Biobased Gel Polymer Electrolytes for Potassium-Ion Conduction. *ACS Applied Polym. Mater.* **2022**, *4*, 3855–3865. [CrossRef]

28. Liu, S.; Kang, L.; Henzie, J.; Zhang, J.; Ha, J.; Amin, M.A.; Hossain, M.S.A.; Jun, S.C.; Yamauchi, Y. Recent advances and perspectives of battery-type anode materials for potassium ion storage. *ACS Nano* **2021**, *15*, 18931–18973. [CrossRef]

29. Wang, Z.; Selbach, S.M.; Grande, T. Van der Waals density functional study of the energetics of alkali metal intercalation in graphite. *RSC Adv.* **2014**, *4*, 3973–3983. [CrossRef]

30. Wu, X.Y.; Leonard, D.P.; Ji, X.L. Emerging non-aqueous potassium-ion batteries: Challenges and opportunities. *Chem. Mater.* **2017**, *29*, 5031–5042. [CrossRef]

31. Eftekhari, A.; Jian, Z.; Ji, X. Potassium secondary batteries. *ACS Appl. Mater. Interfaces* **2017**, *9*, 4404–4419. [CrossRef] [PubMed]

32. Jian, Z.L.; Luo, W.; Ji, X.L. Carbon electrodes for K-ion batteries. *J. Am. Chem. Soc.* **2015**, *137*, 11566–11569. [CrossRef] [PubMed]

33. Wang, W.; Zhou, J.; Wang, Z.; Zhao, L.; Li, P.; Yang, Y.; Yang, C.; Huang, H.; Guo, S. Short-range order in mesoporous carbon boosts potassium-ion battery performance. *Adv. Energy Mater.* **2018**, *8*, 1701648. [CrossRef]

34. Zhang, R.; Li, H.; Li, R.; Wei, D.; Kang, W.; Ju, Z.; Xiong, S. Short-range order in mesoporous carbon boosts potassium-ion battery performance. *Chem. Commun.* **2019**, *55*, 14147–14150. [CrossRef]

35. Lei, Y.; Qui, L.; Liu, R.; Lau, K.C.; Wu, Y.; Zhai, D.; Li, B.; Kang, F. Exploring stability of nonaqueous electrolytes for potassium-ion batteries. *ACS Appl. Energy Mater.* **2018**, *1*, 1828–1833. [CrossRef]

36. Fan, L.; Ma, R.; Zhang, Q.; Jia, X.; Lu, B. Graphite Anode for a Potassium-Ion Battery with Unprecedented Performance. *Angew. Chem. Int. Ed.* **2019**, *58*, 10610–10615. [CrossRef]

37. Fan, L.; Hu, Y.; Rao, A.M.; Zhou, J.; Hou, Z.; Wang, C.; Lu, B. Prospects of electrode materials and electrolytes for practical potassium-based batteries. *Small Methods* **2021**, *5*, 2101131. [CrossRef]

38. Zhang, J.; Lai, L.; Wang, H.; Chen, M.; Shen, Z.X. Energy storage mechanisms of anode materials for potassium ion batteries. *Mater. Today Energy* **2021**, *21*, 100747. [CrossRef]

39. Wang, D.; Tian, K.H.; Wang, J.; Wang, Z.Y.; Luo, S.H.; Liu, Y.G.; Wang, Q.; Zhang, Y.H.; Hao, A.M.; Yi, T.F. Sulfur-doped 3D hierarchical porous carbon network toward excellent potassium-ion storage performance. *Rare Met.* **2021**, *40*, 2464–2473. [CrossRef]

40. Wang, F.; Liu, Y.; Wei, H.J.; Li, T.F.; Xiong, X.H.; Wei, S.Z.; Ren, F.Z.; Volinsky, A.A. Recent advances and perspective in metal coordination materials-based electrode materials for potassium-ion batteries. *Rare Met.* **2021**, *40*, 448–470. [CrossRef]

41. Du, P.; Cao, L.; Zhang, B.; Wang, C.; Xiao, Z.; Zhang, J.; Wang, D.; Ou, X. Recent Progress on Heterostructure Materials for Next-Generation Sodium/Potassium Ion Batteries. *Renew. Sustain. Energy Rev.* **2021**, *151*, 111640. [CrossRef]

42. Yuan, F.; Zhang, W.; Zhang, D.; Wang, Q.; Li, Z.; Li, W.; Sun, H.; Wang, B.; Wu, Y.A. Recent progress in electrochemical performance of carbon-based anodes for potassium-ion batteries based on first principles calculations. *Nanotechnology* **2021**, *32*, 472003. [CrossRef] [PubMed]

43. Ahmed, S.M.; Suo, G.; Wang, W.A.; Xi, K.; Iqbal, S.B. Improvement in potassium ion batteries electrodes: Recent developments and efficient approaches. *J. Energy Chem.* **2021**, *62*, 307–337. [CrossRef]

44. Zhang, W.; Yin, J.; Wang, W.; Bayhan, Z.; Alshareef, H.N. Status of rechargeable potassium batteries. *Nano Energy* **2021**, *83*, 105792. [CrossRef]

45. Ren, X.; Zhao, Q.; McCulloch, W.D.; Wu, Y. MoS$_2$ as a long-life host material for potassium ion intercalation. *Nano Res.* **2017**, *10*, 1313–1321. [CrossRef]

46. Zhang, J.; Cui, P.; Gu, Y.; Wu, D.; Tao, S.; Qian, B.; Chu, W.; Song, L. Encapsulating carbon-coated MoS2 nanosheets within a nitrogen-doped graphene network for high-performance potassium-ion storage. *Adv. Mater. Interfaces* **2019**, *6*, 1901066. [CrossRef]

47. Jiang, Q.; Wang, L.; Chen, J.; Huang, Z.; Yang, H.-J.; Zhou, T.; Hu, J. Enhancing potassium-ion battery performance by MoS2 coated nitrogen-doped hollow carbon matrix. *J. Alloys Compd.* **2021**, *855*, 157505. [CrossRef]

48. Zhou, Y.; Han, Q.; Liu, Y.; Wang, Y.; Jiang, F.; Wang, N.; Bai, Z.; Dou, S. Molybdenum chalcogenides based anode materials for alkali metal ions batteries: Beyond lithium ion batteries. *Energy Storage Mater.* **2022**, *50*, 308–333. [CrossRef]

49. Rehman, J.; Fan, X.; Laref, A.; Dinh, V.A.; Zheng, W.T. Potential anodic applications of 2D MoS$_2$ for K-ion batteries. *J. Alloy. Compd.* **2021**, *865*, 158782. [CrossRef]

50. Choi, J.H.; Park, G.D.; Kang, Y.C. Potassium-ion storage mechanism of MoS2-WS2-C microspheres and their excellent electrochemical properties. *Chem. Eng. J.* **2021**, *408*, 127278. [CrossRef]

51. Chong, S.; Sun, L.; Shu, C.; Guo, S.; Liu, Y.; Wang, W.; Liu, H.K. Chemical bonding boosts nano-rose-like MoS2 anchored on reduced graphene oxide for superior potassium-ion storage. *Nano Energy* **2019**, *63*, 103868. [CrossRef]

52. Hosaka, T.; Matsuyama, T.; Kubota, K.; Tatara, R.; Komaba, S. KFSA/glyme electrolytes for 4 V-class K-ion batteries. *J. Mater. Chem. A* **2020**, *8*, 23766–23771. [CrossRef]

53. Madec, L.; Gabaudan, V.; Gachot, G.; Stievano, L.; Monconduit, L.; Martinez, H. Paving the way for K-ion batteries: Role of electrolyte reactivity through the example of Sb-based electrodes. *ACS Appl. Mater. Interfaces* **2018**, *10*, 34116–34122. [CrossRef] [PubMed]

54. Okoshi, M.; Yamada, Y.; Komaba, S.; Yamada, A.; Nakai, H. Theoretical analysis of interactions between potassium ions and organic electrolyte solvents: A comparison with lithium, sodium, and magnesium ions. *J. Electrochem. Soc.* **2017**, *164*, A54–A60. [CrossRef]

55. Hosaka, T.; Komaba, S. Development of Nonaqueous Electrolytes for High-Voltage K-Ion Batteries. *Bull. Chem. Soc. Jpn.* **2022**, *95*, 569–581. [CrossRef]

56. Na, J.H.; Kang, Y.C.; Park, S.K. Electrospun MOF-based ZnSe nanocrystals confined in N-doped mesoporous carbon fibers as anode materials for potassium ion batteries with long-term cycling stability. *Chem. Eng. J.* **2021**, *425*, 131651. [CrossRef]

57. Wang, B.; Peng, Y.; Yuan, F.; Liu, Q.; Sun, L.; Zhang, P.; Wang, Q.; Li, Z.; Wu, Y.A. A comprehensive review of carbons anode for potassium-ion battery: Fast kinetic, structure stability and electrochemical. *J. Power Sources* **2021**, *484*, 229244. [CrossRef]

58. Dong, X.; Xing, Z.; Zheng, G.; Gao, X.; Hong, H.; Ju, Z.; Zhuang, Q. MoS$_2$/N-doped graphene aerogles composite anode for high performance sodium/potassium ion batteries. *Electrochim. Acta* **2020**, *339*, 135932. [CrossRef]

59. Bella, F.; Verna, A.; Gerbaldi, C. Patterning dye-sensitized solar cell photoanodes through a polymeric approach: A perspective. *Mater. Sci. Semicond. Process.* **2018**, *73*, 92–98. [CrossRef]

60. Bella, F.; Popovic, J.; Lamberti, A.; Tresso, E.; Gerbaldi, C.; Maier, J. Interfacial effects in solid–liquid electrolytes for improved stability and performance of dye-sensitized solar cells. *ACS Appl. Mater. Interfaces* **2017**, *9*, 37797–37803. [CrossRef]

61. Bella, F.; Lamberti, A.; Bianco, S.; Tresso, E.; Gerbaldi, C.; Pirri, C.F. Floating Photovoltaics: Floating, Flexible Polymeric Dye-Sensitized Solar-Cell Architecture: The Way of Near-Future Photovoltaics. *Adv. Mater. Technol.* **2016**, *1*, 1600002. [CrossRef]

62. Gerosa, M.; Sacco, A.; Scalia, A.; Bella, F.; Chiodoni, A.; Quaglio, M.; Tresso, E.; Bianco, S. Toward totally flexible dye-sensitized solar cells based on titanium grids and polymeric electrolyte. *IEEE J. Photovoltaics* **2016**, *6*, 498–505. [CrossRef]

63. Sacco, A.; Bella, F.; de la Pierre, S.; Castellino, M.; Bianco, S.; Bongiovanni, R.; Pirri, C.F. Electrodes/electrolyte interfaces in the presence of a surface-modified photopolymer electrolyte: Application in dye-sensitized solar cells. *ChemPhysChem* **2015**, *16*, 960–969. [CrossRef] [PubMed]

64. Veeramalai, C.P.; Li, F.; Liu, Y.; Xu, Z.; Guo, T.; Kim, T.W. Enhanced field emission properties of molybdenum disulphide few layer nanosheets synthesized by hydrothermal method. *Appl. Surf. Sci.* **2016**, *389*, 1017–1022. [CrossRef]